International Journal of Material Forming (2019) 12:1–15
https://doi.org/10.1007/s12289-018-1398-3

ORIGINAL RESEARCH

A methodology for determining preform compaction in bladder-assisted resin transfer molding with elastomeric bladders for tubular composite parts

Christian Schillfahrt[1] · Ewald Fauster[1] · Ralf Schledjewski[1]

Received: 15 August 2017 / Accepted: 2 January 2018 / Published online: 15 January 2018

Abstract
A common approach for the manufacturing of hollow composite parts based on textile reinforcement materials is the utilization of bladder-assisted resin transfer molding (BARTM). Here, the process-induced compaction of the preform is a decisive factor in the injection stage as it significantly influences filling times and part qualities. However, the use of expandable elastomeric bladders impedes the determination of local compaction pressures and thicknesses of compliant preforms during BARTM. This paper therefore presents an efficient methodology for evaluating the compaction state of tubular fabrics during preform compaction and subsequent resin injection by considering the membrane stiffness of an elastomeric bladder as well as the compressibility of the textile preform. First, different process models are developed to describe preform compaction based on single-point and full preform compaction data. The acquisition of exemplary model data for bladder expansion and preform compaction is accomplished through experimental methods. A specifically developed test rig comprising optical measurement techniques is used to directly characterize the radial expansion behavior of tubular silicone rubber bladders. The compaction behavior of single- and multi-layered braided preforms is evaluated by means of dry compression experiments. The resulting measurement data is used to create an integral model-based process window for combined bladder expansion and preform compaction. Lastly, a prediction of relevant local compaction pressures and preform thicknesses is conducted for an exemplary BARTM process.

Keywords Resin transfer molding · Bladder inflation molding · Elastomeric bladder · Process modeling · Preform compaction · Part thickness

Introduction

Bladder-assisted resin transfer molding (BARTM) represents a special process technology for the manufacturing of hollow composite structures based on fiber reinforced plastics (FRP). As with any other liquid composite molding (LCM) methods, the basic process principle comprises the impregnation of a stack of dry reinforcing textiles positioned inside a closed mold with a liquid polymer matrix, which is injected under a specific fluid pressure or flow rate [1]. In contrast to process variants that solely use rigid mold components, BARTM typically uses a rigid, two-part outer mold and an internal flexible bladder. The latter can be inflated by air or fluid pressure in order to compress the externally positioned fabrics against the outer mold [2, 3]. After ensuring a certain degree of preform compaction, the injection of the impregnating resin is conducted in a subsequent process step. Normally, a constant ratio of the counteracting bladder and injection pressures is maintained throughout preform saturation [4]. Following the filling stage, the bladder pressure can be increased in a so-called consolidation step in order to compensate laminate thickness variations and to drain excessive resin [5]. Obviously, preform compaction represents a decisive factor in BARTM as it substantially influences process- and quality-related parameters such as filling time, part thickness and fiber volume content [6].

For the fabrication of rather longish composite parts, such as fluid piping elements or frame structures, flexible tube-like bladders in combination with tubular fabrics are typically

✉ Ewald Fauster
ewald.fauster@unileoben.ac.at

[1] Processing of Composites Group, Department of Polymer Engineering and Science, Montanuniversität Leoben, Otto Glöckel-Straße 2/III, 8700 Leoben, Austria

used. The choice of the appropriate bladder type usually is a difficult task. Apart from economic demands, it can depend on various process-related aspects [5, 7]:

- Mechanical and thermal stability to withstand process pressures and temperatures during BARTM while providing complete gas or fluid tightness against the internal pressure medium,
- ability of the bladder to fully conform to the internal part geometry, in order to prevent race tracking effects during injection and the formation of resin-rich areas in the laminate,
- deformability of the bladder to realize complex shapes without the formation of wrinkles in order to ensure a smooth internal part surface,
- removability of the bladder in order to fully exploit the lightweight potential of the final composite structure,
- adhesion to the matrix if the bladder is intended to remain on the internal surface of the part, where it can act as an additional functional layer (e.g. for chemical resistance or gas tightness),
- reusability of the bladder, and
- inherent stability of the bladder to facilitate preform manufacturing and handling (e.g. if the bladder is directly used as a mandrel in an over-braiding process).

A basic classification of bladder types in terms of dimensional and mechanical aspects is given in Fig. 1. Under-sized bladders need to be radially expanded to enable preform compaction, either based on an elastic or plastic deformation of the membrane (Fig. 2a) [3, 5]. If the tubular fabrics are directly applied to the bladder surface, a sufficiently high degree of preform drapability is required. Depending on the initial bladder dimension, preforms with variable thicknesses can be used, which is beneficial for a flexible small-scale production. While elastically expandable bladders can be reused in the process, the influence of their mechanical properties on preform compaction due to the formation of pressure-induced membrane stresses should be considered [8]. In contrast, exact-sized bladders facilitate the utilization of near-net shape preforms and omit the need of a subsequent draping of the textile reinforcements (Fig. 2b). However, a major drawback of this approach is that fiber pinching, describing the trapping of fibers between the closing mold halves, can occur, which can be prevented using complex but costly tool designs [5, 9]. Over-sized bladders typically consist of rather thin-walled tubular membranes (Fig. 2c). They are unfolded during bladder inflation and can adapt to a large range of cross-sectional shapes and dimensions [7]. A stretchable membrane material is beneficial if angular cross-sections have to be molded [5]. However, preform preparation and handling using these bladders is difficult. Furthermore, wrinkle formation in the membrane impedes the realization of a smooth inner part surface.

The compaction behavior of textile preforms has been extensively studied in the last decades. Dry reinforcement materials consisting of interlaced fibers, such as woven or braided fabrics, typically show significant compliance in the transverse direction mainly due to their characteristic out-of-plane yarn waviness [10]. Preform thickness and fiber volume fraction are directly affected by the transverse compaction pressure applied during processing, which usually follows a highly non-linear relationship. The major influencing factors contributing to the preform compaction behavior are yarn cross-section deformation, yarn flattening (i.e. decrease of fiber crimp), yarn bending deformation, intra-yarn void condensation and nesting [6, 10]. The latter one only occurs in multi-layer preforms and depends on various textile parameters such as the binding pattern, degree of shear and number of layers [11–13]. Moreover, it was shown that preform compaction is time dependent, non-elastic and influenced by the presence of a saturating fluid causing lubrication effects that facilitate reorganization of the fiber network [14–16]. Although some authors have made considerable efforts in compaction modelling of textile preforms based on force, energy or finite element approaches, preform compliance is still widely characterized by means of experimental compression tests and analytically described using empirical compaction models [10, 11, 17, 18].

The influence of bladder type and material on preform compaction during BARTM is not yet fully explored in the literature and only few works are available. Lehmann and Michaeli [4, 5] investigated different under-sized and near-net shape bladders suited for BARTM by evaluating the bladder pressures required to fully adapt to a rectangular-shaped mold geometry. Although they conducted preliminary tests also using elastomeric bladders, they later focused on thin-walled thermoplastic tubular films that were plastically preexpanded to a near-net shape. Thus, it was assumed that no membrane stresses occur during BARTM. Their effect on preform compaction for the resin injection stage was therefore neglected. Strohhäcker [7] studied various thermoplastic and elastomeric bladders for thermoplastic bladder inflation molding of fabrics consisting of hybrid yarns. However, he ignored the effect of under-sized elastically expanded bladders on preform compaction. Bezerra et al. [19] investigated the expansion behavior of prefabricated composite tubes impregnated with a b-staged resin using an inflatable silicone rubber bladder and a mold showing cylindrical and conical regions. They considered the influence of the under-sized elastomeric bladder on

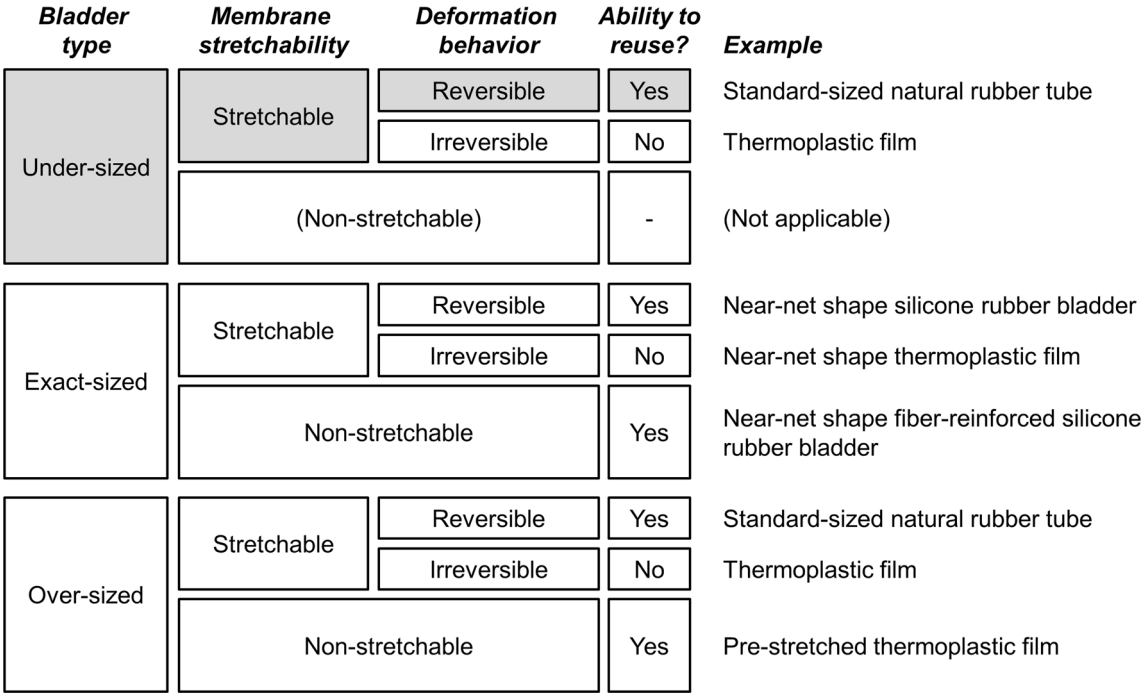

Fig. 1 Classification of bladder types for BARTM in terms of dimensional and mechanical aspects. The bladder type investigated in the present work is highlighted

preform compaction by monitoring the internal bladder pressure and by using a contact sensor based on a chip antenna. However, due to the conical shape of the mold cavity, the determined bladder pressure required for material contact as well as the compaction pressure is valid only for the given sensor position. Fong et al. [20] investigated a resin transfer molding process comprising both rigid and flexible mold walls. They developed a mathematical deformation model for an elastomeric mold wall, but by assumption of a thin-walled highly compliant membrane material, the rigidity of the bladder and its impact on compaction was neglected. Preform compaction during vacuum-assisted resin infusion (VARI), a process technically similar to BARTM, was intensively studied in the literature, but the influence of the membrane is generally neglected due to the absence of membrane stresses [16, 21, 22]. In previous work of the authors [8], the filling behavior of tubular braided fabrics in BARTM was investigated by means of a specifically developed saturation test rig, in which the preform is compressed using an under-sized silicone rubber bladder. A simple compaction model was proposed for analyzing local compaction pressures during resin injection, which considered the influence of the bladder through a separate model parameter. However, no procedure was given for the determination of this parameter. Moreover, preform compliance was generally neglected in this model.

In contrast to the aforementioned studies, this paper presents an efficient methodology for evaluating the process-induced preform compaction pressure and thickness at the injection gate and flow front during BARTM. Due to the complexity and variety of different process variants, the following work is focused on a specific application case. It addresses the manufacturing of a cylindrical composite part by considering the membrane stiffness of an under-sized elastomeric bladder as well as the compressibility of a tubular preform with high

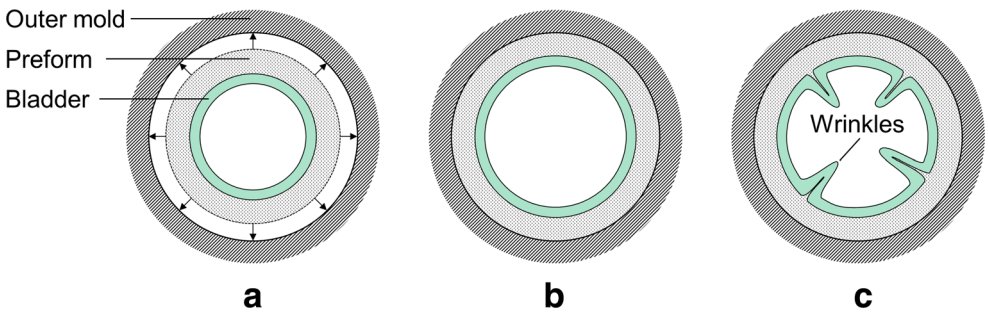

Fig. 2 Cross-sectional view of different bladder types for an exemplary tubular BARTM setup: (**a**) Under-sized, (**b**) exact-sized and (**c**) over-sized bladder

diameter-to-thickness ratio. Preliminary tests showed, that direct measurement of the preform compaction pressure inside a rather small tubular BARTM assembly, for example by the use of pressure sensitive films or force sensing resistors, is a complex task. Poor measuring accuracy, difficult integration particularly for wired sensors, influence on fluid flow and high sensor costs are considered as major limitations. Therefore, a different approach is proposed in the present work:

- At first, a preform compaction model for a tubular BARTM setup is developed in the theoretical section, which relates the applied bladder and injection pressure with the resulting preform compaction pressure. The process model integrates the interdependent effects of bladder expansion and fabric compression considering different types of preform compaction behavior.
- The experimental work is focused on the determination of exemplary model data for bladder expansion and preform compaction. Regarding the former, a novel optical test method is proposed to characterize the radial expansion behavior of tubular silicone rubber bladders. Evaluation of preform compliance is accomplished by means of a conventional compaction test rig at the example of single- and multi-layered braided fabrics.
- The experimental data is used to create a process window for combined bladder expansion and preform compaction as well as to compute relevant local compaction pressures and preform thicknesses based on an exemplary BARTM process. The results of the different compaction models are finally compared and discussed.

Theoretical background

Preform compaction prior to resin injection

In this section the basic relationships for the radial expansion of an under-sized elastomeric bladder and the resulting preform compaction are given for the following cases:

- a theoretically incompressible preform (model P1),
- a compressible preform with compressibility neglected beyond a specific level of compaction pressure (model P2), and
- a compressible preform considering its full compressive behavior (model P3).

Initially an incompressible preform showing a constant thickness $h_{p,\ 0}$ is considered. In Fig. 3 the relevant stages of preform compaction in a tubular BARTM setup are depicted. At first, the under-sized bladder is inflated and radially expanded by application of an internal bladder pressure p_b (Fig. 3a). For this work, it is assumed that bladder expansion is not hindered by the externally positioned preform, which implies that (a) there is no mechanical interaction between the bladder and the textile reinforcement, (b) the preform can be radially expanded without significant force or (c) the preform does not need to be expanded. Hence, no stresses are induced in the orthotropic reinforcement material during the bladder expansion stage. This assumption may be valid e.g. for near-net shape preforms, for flat fabrics that are loosely wound around the bladder or for biaxial braided fabrics with rather low braid angles. However, some preforms such as braided fabrics with high braid angles can hinder bladder expansion due to high frictional forces or locking of the interlaced reinforcing yarns [23]. Thus, prior investigation of the fabric's drapability and jamming condition through experimental tests [24, 25] or draping models [23, 26] is recommended, but is out of scope of this paper. When the minimum pressure for full radial bladder expansion $p_{b,\ min}$ is reached, the preform is in full contact with both the bladder and the outer mold (Fig. 3b). Any further increase of bladder pressure will compress the externally positioned fabrics against the outer mold (Fig. 3c), which results in a growing preform compaction pressure p_c given by:

$$p_c = p_b - p_{b,min} \quad for \quad p_b > p_{b,min}, \text{while} \tag{1}$$

$$p_c = 0 \quad for \quad p_b \leq p_{b,min}. \tag{2}$$

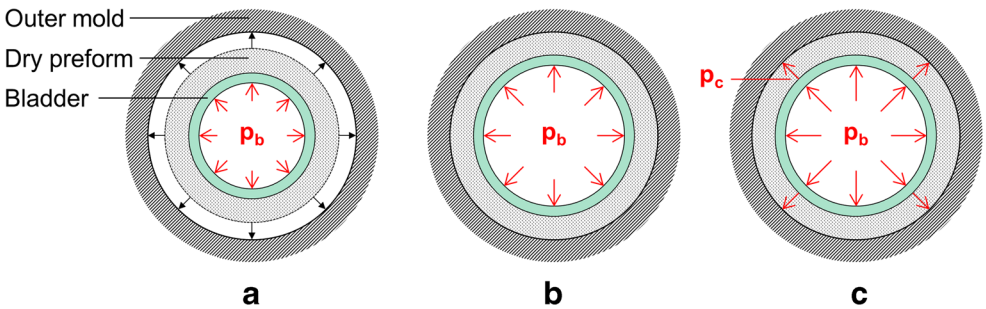

Fig. 3 Cross-sectional view of the relevant stages of preform compaction prior to resin injection: (**a**) Pressure-induced bladder expansion ($0<p_b<p_{b,\ min}$), (**b**) mold contact of preform ($p_b=p_{b,\ min}$) and (**c**) compaction ($p_b>p_{b,\ min}$) of the dry reinforcement material inside a cylindrical mold

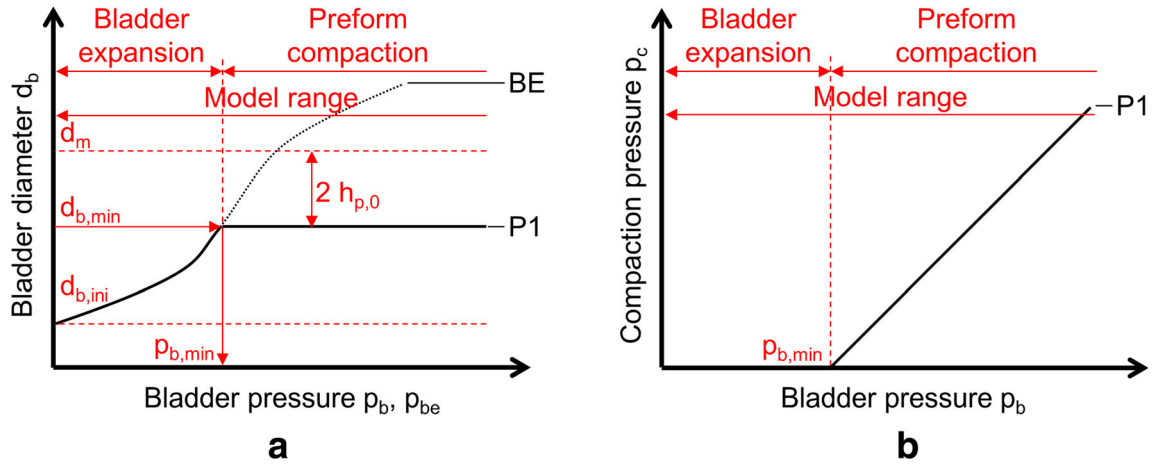

Fig. 4 Process windows for bladder expansion and preform compaction for an incompressible preform, where (**a**) the outer bladder diameter and (**b**) the preform compaction pressure is plotted against the internal bladder pressure. BE terms the stand-alone bladder expansion behavior, while P1 denotes the combined bladder-preform-behavior

The pressure $p_{b,\ min}$ considers the stiffness of the internal elastomeric bladder, which decreases the transmitted compaction pressure to the preform. This parameter can be determined either by the use of sensors for detecting mold contact or monitoring compaction pressure [19], or by evaluating the radial expansion behavior of the outer bladder diameter d_b in order to compute the unknown pressure parameter $p_{b,\ min}$ by:

$$p_{b,min} = p_{be}\left(d_b = d_{b,min}\right), \tag{3}$$

where $p_{be}(d_b)$ denotes the stand-alone bladder expansion curve that can be obtained either from a pressure-controlled bladder expansion measurement or from FE analysis using an appropriate hyperelastic material model. Knowing the cavity diameter d_m of the outer mold as well as the preform thickness $h_{p,\ 0}$, the outer bladder diameter $d_{b,\ min}$ at full radial expansion can be expressed as:

$$d_{b,min} = d_m - 2h_{p,0} \tag{4}$$

and obviously corresponds to the inner preform diameter. Hence, $p_{b,\ min}$ can be predicted for different mold and preform dimensions if the bladder expansion curve, which is influenced by the material properties and initial dimensions of the bladder, is known. For an incompressible preform, the outer bladder diameter d_b of the BARTM setup during the compaction phase is given by:

$$d_b = d_{b,min} \quad for \quad p_b > p_{b,min}, \text{while} \tag{5}$$

$$d_b = f(p_b) = f(p_{be}) \quad for \quad p_b \leq p_{b,min}. \tag{6}$$

In conclusion, Fig. 4 shows the process windows of model P1 for bladder expansion and preform compaction prior to resin injection.

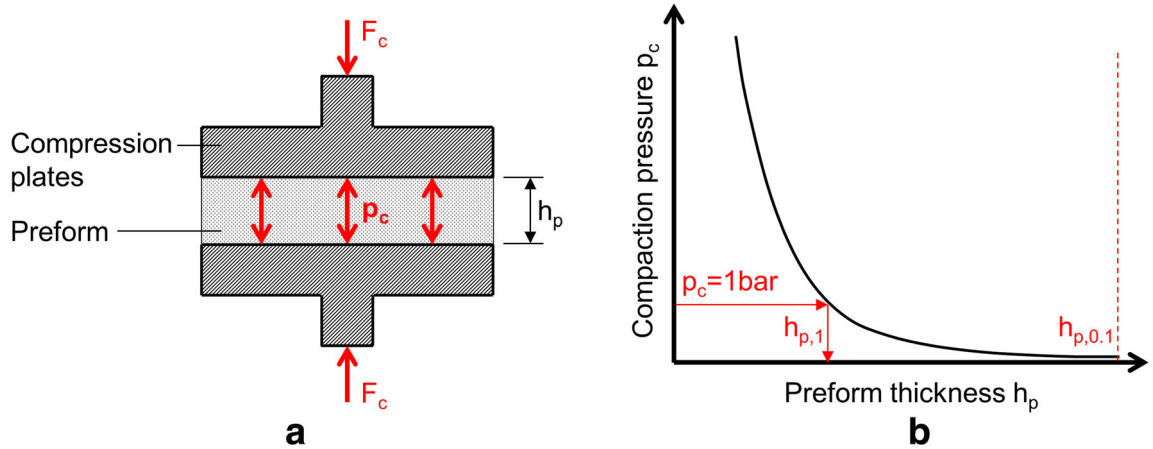

Fig. 5 Evaluation of preform compressibility: (**a**) Schematic test setup, consisting of two compression plates with defined dimensions loaded with a compressive force F_c in order to adjust a desired preform compaction pressure p_c and (**b**) typical resulting preform compaction curve

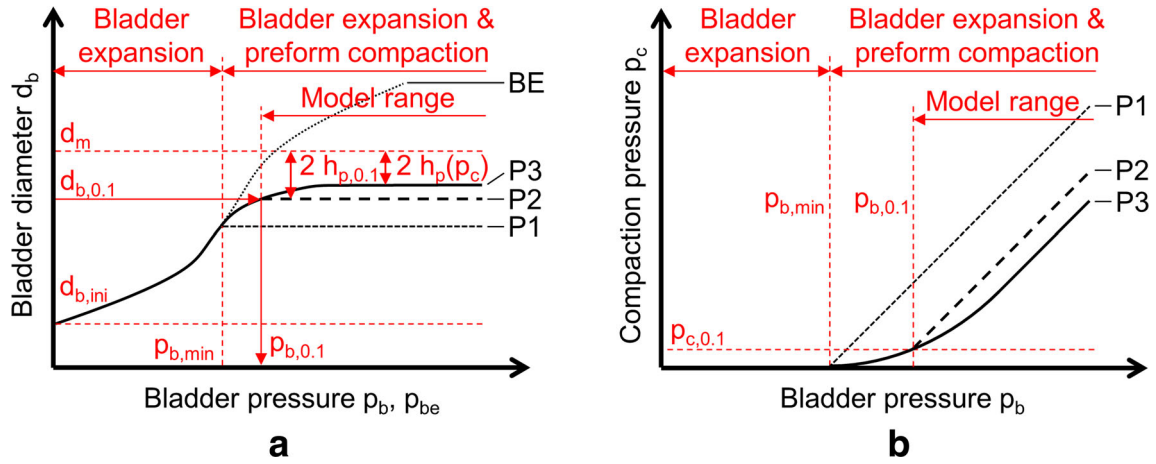

Fig. 6 Process windows for bladder expansion and preform compaction for a compressible preform, where (**a**) the outer bladder diameter and (**b**) the preform compaction pressure is plotted against the internal bladder pressure. P2 and P3 denote the combined bladder-preform- behavior without and with consideration of preform compressibility for $p_b \geq p_{b,0.1}$. P1 describes the combined model of an incompressible preform and BE terms the stand-alone bladder expansion behavior

If the preform thickness decreases significantly for increasing compaction pressures, then the compressibility of the preform and its effect on preform compaction due to further bladder expansion should be considered. In contrast to incompressible preforms, the initial thickness of an unloaded compressible preform $h_{p,\,0}$ is difficult to determine and usually unknown [14]. Consequently, according to Eqs. (3) and (4), also $p_{b,\,min}$ and $d_{b,\,min}$ cannot be evaluated. In practice, the initial preform thickness is commonly evaluated for a specific minimum compaction pressure, e.g. by using a weight-loaded fabric thickness gauge. In this work, the preform thickness $h_{p,\,0.1}$ is determined for a minimum compaction pressure $p_{c,\,0.1}$ of 0.1 bar, which corresponds to an internal bladder pressure $p_{b,\,0.1}$ of the BARTM setup. This parameter may be chosen to coincide with a specific minimum compaction pressure in order to prevent flow-induced fiber displacement during resin injection. The followed concept of model P2 is that any further thickness change for $p_b > p_{b,\,0.1}$ is neglected, which minimizes the effort for preform compressibility characterization by using single-point compaction data (i.e. $p_{c,\,0.1}$, $h_{p,\,0.1}$) only. The preform compaction pressure can be expressed as:

$$p_c = p_b - p_{b,0.1} + p_{c,0.1} = p_b - p_{be,0.1} \quad \text{for} \quad p_b \geq p_{b,0.1}, \tag{7}$$

where the pressure parameter $p_{be,\,0.1}$, which represents the pressure portion that is solely responsible for radial bladder expansion, can be determined similar to the abovementioned procedure by:

$$p_{be,0.1} = p_{be}\left(d_b = d_{b,0.1}\right), \text{and} \tag{8}$$

$$d_{b,0.1} = d_m - 2h_{p,0.1}, \text{while} \tag{9}$$

$$d_b = d_{b,0.1} \quad \text{for} \quad p_b \geq p_{b,0.1}, \tag{10}$$

where $d_{b,\,0.1}$ denotes the inflated bladder diameter for a preform compaction of 0.1 bar. It has to be noted that due to the uncertainty of $p_{b,\,min}$, the applicable range of model P2 is limited to bladder pressures greater than $p_{b,\,0.1}$.

Alternatively, the exact thickness change of the preform can be considered by knowing its compaction behavior $p_c(h_p)$. This

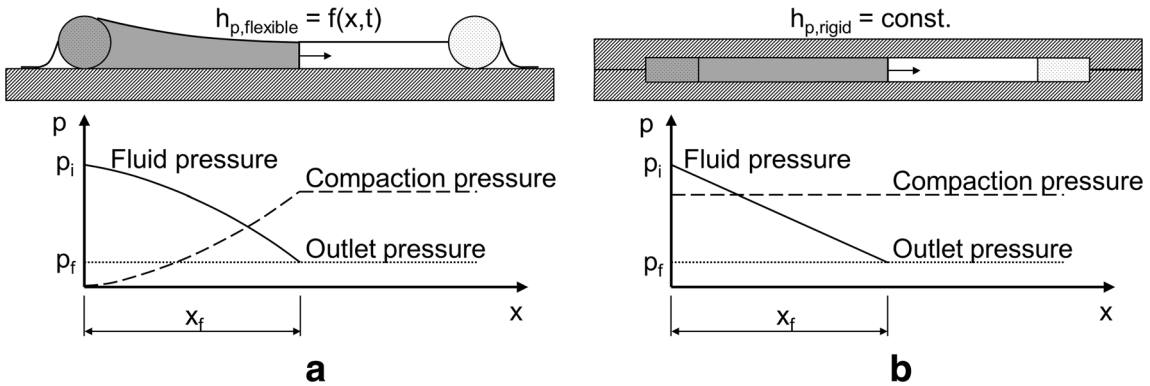

Fig. 7 Process illustrations and relevant pressure profiles of (**a**) a flexible mold process, such as VARI or BARTM, in comparison with (**b**) a rigid mold process, such as RTM [8]

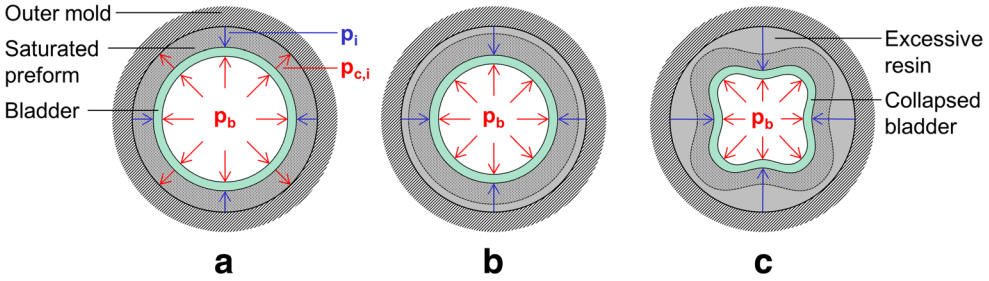

Fig. 8 Cross-sectional view of different process conditions at the injection point during BARTM: (**a**) Maintenance of preform compaction (p_b-p_i>$p_{b,\,min}$), (**b**) loss of preform compaction due to contracting bladder ($0 \leq p_b$-$p_i \leq p_{b,\,min}$) and (**c**) pressure-induced collapsing of the bladder (p_b-p_i<0)

in turn can be simply obtained by a planar compression test (Fig. 5), if a sufficiently high diameter-to-thickness ratio of the tubular preform is given. Again, the initial maximum preform thickness is chosen to be practically limited by $h_{p,\,0.1}$. Consequently, for $p_b \geq p_{b,\,0.1}$, the internal bladder pressure applied on the BARTM setup is composed of a pressure portion p_{be} responsible for bladder expansion until a certain preform thickness is reached and a pressure portion corresponding to the respective preform compaction pressure:

$$p_b = p_{be}\left(d_b\left(h_p\right)\right) + p_c\left(h_p\right) \quad \text{for} \quad p_b \geq p_{b,0.1}. \tag{11}$$

It has to be noted that this implicit model equation has to be solved using numerical methods in order to determine the preform thickness h_p as well as the corresponding preform compaction pressure and outer bladder diameter for a given internal bladder pressure. The process windows for bladder expansion and preform compaction of model P2 and P3 are illustrated in Fig. 6.

In order to mathematically describe the compaction behavior of the textile preform, an empirical power-law approach is used in this work. This is widely reported in literature for woven and braided fabrics assuming that preform compaction is not time dependent [5, 14, 15, 21, 27–29]:

$$\varphi = \varphi_1 {p_c}^B, \tag{12}$$

where φ terms the fiber volume fraction (FVF), φ_1 is the FVF at the unit compaction pressure (1 bar in this work) and B denotes the stiffening index, which is reported to have a value smaller than 1. FVF can also be expressed by [21]:

$$\varphi = \frac{G}{\rho_f h_p}, \tag{13}$$

where ρ_f is the fiber density, while G and h_p correspond to the grammage and actual thickness of the preform. Combining Eq. (12) and (13) results in:

$$p_c = \left(\frac{h_{p,1}}{h_p}\right)^{1/B} \text{for } h_p \leq h_{p,0.1}, \tag{14}$$

where $h_{p,\,1}$ terms the preform thickness at a compaction pressure of 1 bar (Fig. 5b).

Preform compaction during resin injection

Resin injection processes comprising flexible molds, including VARI and BARTM, exhibit a non-linear fluid pressure profile along the flow length, which in turn is inversely proportional to the preform compaction pressure, as depicted in Fig. 7 [5, 16, 20–22, 30]. This effect is caused by the compressibility of the preform in conjunction with the

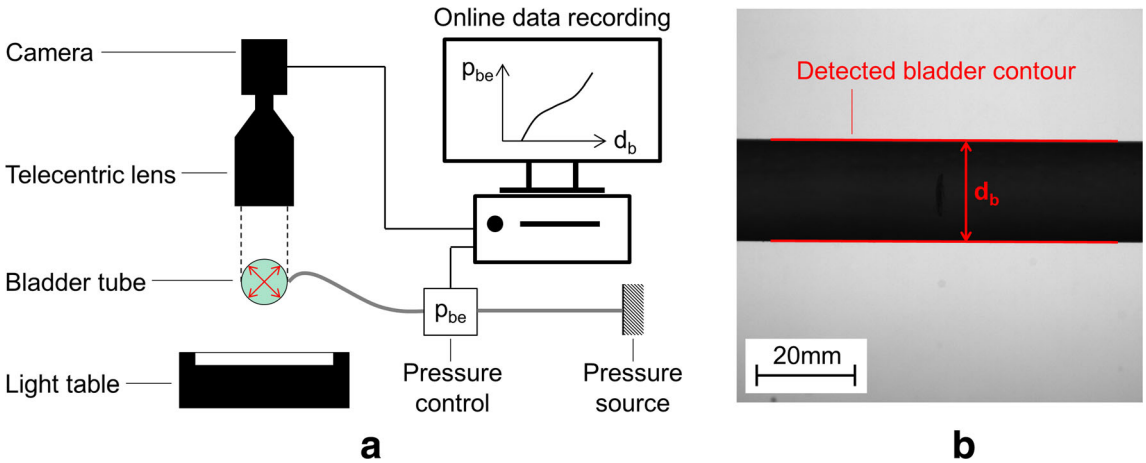

Fig. 9 Optical bladder diameter measurement: (**a**) Test setup and (**b**) exemplary analysis

Table 1 Relevant parameters of the tested bladder tube specimens

Parameter	Value or designation
Bladder material	Silicone rubber tube, Shore A 60
Inner / outer bladder diameter (mm)	12 / 15
Specimen length (mm)	400

deformability of the flexible mold part [21]. The compaction pressure field during BARTM can be roughly described by two relevant boundary parameters: the compaction pressure $p_{c,\,i}$ at the fluid inlet position and the constant pressure $p_{c,\,f}$ in the section between the flow front and the outlet position. While the former is significantly dependent on the counteracting fluid injection pressure p_i at the inlet, the latter can be influenced by the relative outlet pressure p_f acting on the fluid flow front and the unsaturated preform region (e.g. p_f=0 for BARTM at atmospheric pressure or p_f= − 1 bar for vacuum-assisted BARTM). Hence, the effective bladder pressures $p_{b,\,i}$ and $p_{b,\,f}$ have to be used instead of p_b in Eqs. (1), (7) and (11) in order to calculate the locally applied compaction pressures $p_{c,\,i}$ and $p_{c,\,f}$ during resin injection:

$$p_{b,i} = p_b - p_i, \tag{15}$$

$$p_{b,f} = p_b - p_f. \tag{16}$$

Regarding the abovementioned relationships for compressible preforms, it should be noted that compaction properties during resin injection can differ from those found in unsaturated conditions due to compaction hysteresis and lubrication effects [16, 21, 22, 30]. Ideally, different compaction data should be used for describing dry preform compaction and subsequent wet decompaction. This work, however, involves only dry compaction data for illustration purposes.

A decisive factor in BARTM is the maintenance of a certain amount of preform compaction during fluid injection. This helps avoiding or minimizing effects such as fiber washout, fabric distortion, preform thickness evolution and bladder collapsing, particularly at the inlet position [5, 31, 32]. Here, the following relation has to be fulfilled throughout the injection process to maintain a minimum degree of compaction pressure, i.e. $p_c \geq p_{c,\,0.1}$:

$$p_b - p_i \geq p_{b,0.1}. \tag{17}$$

If this condition is violated, the following cases can occur (Fig. 8):

- $p_{b,\,min} < p_b - p_i < p_{b,\,0.1}$: Preform compression falls below minimum compaction pressure, which results in increasing preform thickness evolution and possible flow-induced fiber displacement.
- $0 \leq p_b - p_i \leq p_{b,\,min}$: Loss of compaction as the bladder will locally contract until its initial dimension is reached, leading to an introduction of excessive resin and a significant decrease in FVF.
- $p_b - p_i < 0$: Bladder can collapse due to high injection pressure.

Some of the above cases may have its application in accelerating the fluid injection process [20]. In this work however, we only consider conditions where Eq. (17) is satisfied. Moreover, preform compaction and consolidation subsequent to the injection stage due to post-filling fluid flow [33, 34] and resin bleeding [35] is not addressed here.

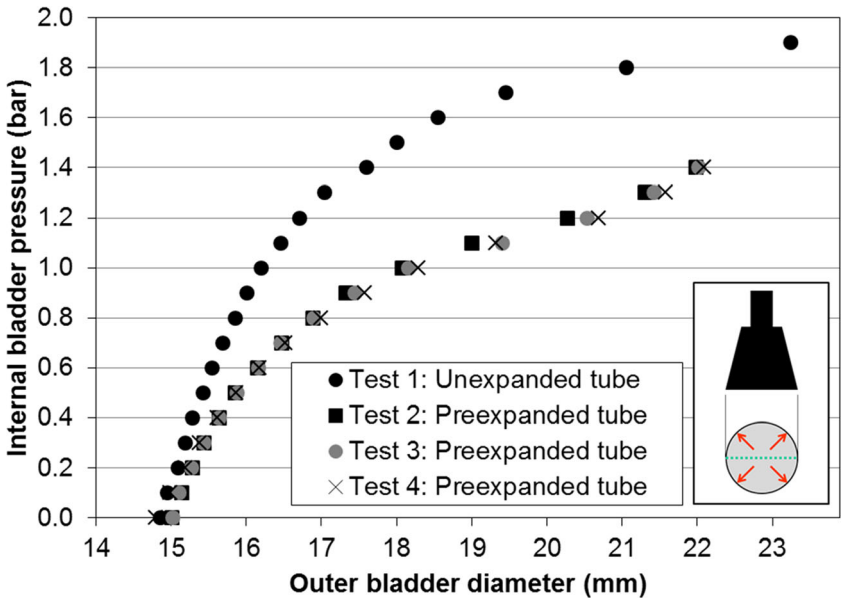

Fig. 10 Repetitive optical bladder expansion measurements of an unused silicone rubber tube

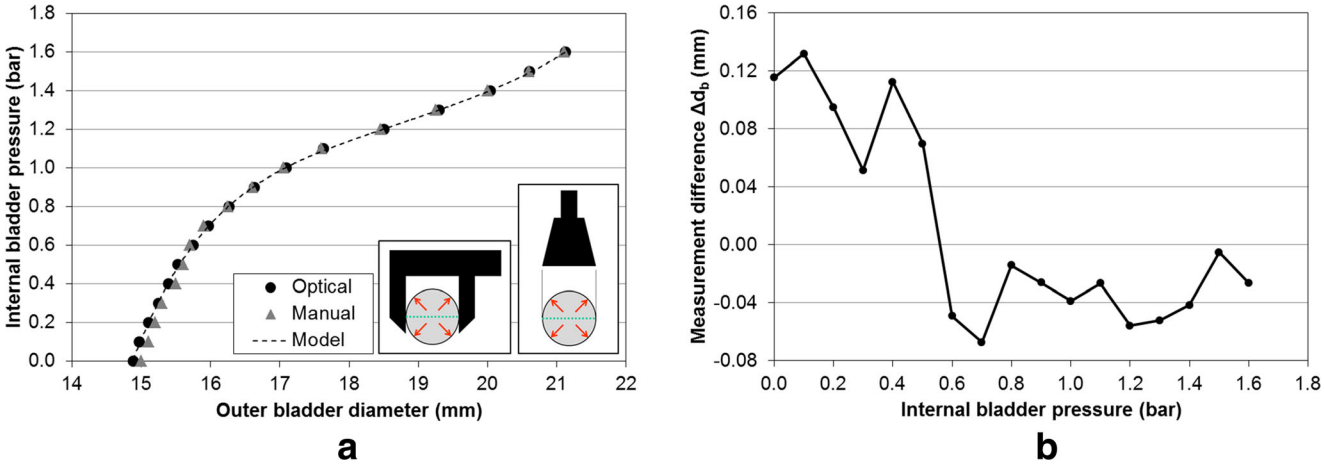

Fig. 11 Bladder expansion measurement of a preexpanded silicone rubber tube: (a) Optically detected and modeled outer bladder diameters compared to manually obtained measurements; (b) Differences in diameter between the manual and optical measurement method over the applied bladder pressure

Bladder expansion measurement

Test rig

In contrast to a comprehensive development of a hyperelastic material model in order to describe the deformation behavior of an elastomeric tube, an application-oriented bladder characterization is beneficial in terms of measurement and computation effort. Thus, the basic approach followed here is to design a fast and simple method to directly characterize the radial expansion behavior of a tubular non-reinforced elastomeric bladder prior to its use in BARTM. A specifically developed test rig comprising a monochromatic camera equipped with a telecentric lens and a light table for background illumination was constructed (Fig. 9). In between, the bladder to be characterized is positioned, which is equipped with connector elements at both ends and connected to a compressed air supply comprising a digital pressure controller. In order to avoid any off-axis deformation of the test specimen, one of the two connector elements is mounted to allow for free motion in longitudinal direction, which is caused by a pressure-induced elongation of the bladder. All electrical components are attached to a control and measurement system involving a LabView application enabling a fully automated testing procedure. The online analysis of the actual bladder diameter is accomplished by means of efficient digital image processing techniques. The basic idea is to find the positions of high intensity gradients in predefined regions of interest along the contour lines of the bladder. The resulting data sets are separated into two groups, one for each contour line, and approximated by a pair of parallel lines. Finally, the tube diameter can be determined as the orthogonal distance between these two lines. Transfer of the result to a metric scale involves a scaling factor determined from a preceding calibration. Due to the use of a telecentric lens, the optical resolution of the test system is independent of the measurement distance and is about 0.085 mm/pixel. The measurement resolution is somewhat higher as the software algorithm enables measurements with subpixel accuracy.

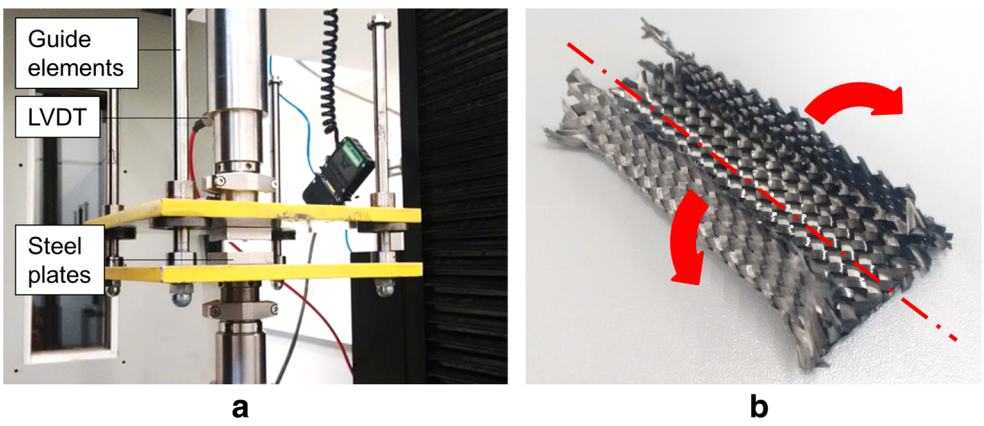

Fig. 12 Preform compaction measurement: (**a**) Test setup and (**b**) specimen preparation by means of cutting, opening and flattening of a specifically draped tubular braid

Table 2 Relevant parameters of the braided fabric

Parameter	Value or designation
Material type	Carbon
Binding pattern	Diamond
Filament count	12 K
Filament diameter (μm)	7
Number of strands	36
Nominal diameter at ±45° (mm)	22.9
Nominal areal weight at ±45° (g/m^2)	566
Actual braid angle (°)	±38
Actual areal weight (g/m^2)	584

In order to perform an optical bladder expansion measurement, the tube to be tested is inflated by a stepwise increase of the internal pressure. Each pressure plateau is held for a short time to allow an optical measurement of a mean tube diameter by analyzing a captured frame set based on a given image acquisition rate. The measurement sequence is stopped when a predefined outer bladder diameter is reached.

Investigation of the bladder expansion behavior

The bladder expansion measurements are focused on silicone rubber tubes (Table 1). The pressure-controlled tube diameter measurements were conducted at room temperature with a step-size of 0.1 bar, an image acquisition rate of 10 s^{-1} and a recording time of 2 s. The resulting radial bladder expansion profiles of a series of repetitive measurements are illustrated in Fig. 10 and naturally show a highly non-linear behavior. Here, the first measurement of a new unused tube shows a considerably different expansion profile than the ones of the following repetitive measurements. This is caused by the so-called Mullins effect, which describes an irreversible stress-softening of a rubber-like material during cyclic loading. Most importantly, this effect only appears when a maximum previously encountered loading or elongation is exceeded [36]. In this case, the silicone rubber tube was expanded to about 23 mm in diameter during the first measurement. However, as this limit has not been exceeded, similar expansion profiles were obtained for the following measurements.

Based on these findings, the Mullins effect of a reusable elastomeric bladder has to be taken into account to guarantee a reproducible expansion behavior and thus preform compression during BARTM processing. This can be accomplished by an initial bladder preexpansion to a specific maximum tube diameter that cannot be exceeded during the subsequent use in the manufacturing process. The following measurements were therefore conducted using a new bladder tube that has been inflated inside the previously mentioned BARTM test rig [8] to a diameter of 21 mm, which corresponds to the inner diameter of the outer mold.

The optically measured results were verified with manual measurements obtained with a micrometer screw gauge (Fig. 11). In general, good agreement between the results was found, although manual measurements predominantly show slightly smaller values, which can be explained by a possible deformation of the flexible tube during the tactile measurement. Higher deviations at lower bladder pressures are presumably caused by the low internal supporting pressure of the tube, leading the tube to differ from a perfectly round shape and making it sensitive to handling during manual measurement.

Finally, in order to mathematically consider the radial expansion behavior $p_{be}(d_b)$ of the silicone rubber tube in the models P1, P2 and P3 according to Eqs. (3), (8) and (11), respectively, the optically measured expansion profile is adequately fitted with a fifth-order polynomial deformation model (Fig. 11a):

$$p_{be}(d_b) = 0.0002{d_b}^5 - 0.0208{d_b}^4 + 0.8529{d_b}^3 - 17.42{d_b}^2 + 177.6d_b - 722.0 \; for 15 \le d_b \le 21 \text{ mm}. \tag{18}$$

Preform compaction measurement

Experimental procedure

Dry preform compaction measurements are conducted on a 100 kN INSTRON universal testing machine in order to consider the compressive behavior of the textile preform in the corresponding models P2 and P3. The measurement setup comprises two polished steel plates with a pressure-active area A_c=38.65 × 38.00 mm^2 and vertical guiding elements at each corner of the assembly to maintain exact lateral alignment and to avoid tilting of the compression plates (Fig. 12a). A precise measurement of the vertical steel plate displacement, corresponding to the actual preform thickness during testing, is realized by means of a calibrated linear variable differential transformer (LVDT).

Table 3 Testing parameters for the dry compaction experiments

Parameter	Value or designation
Compression rate (mm/min)	0.5
Data acquisition rate	100 ms OR 10 N
Minimum compressive load (N)	5 (≙ 0.03 bar)
Maximum compressive load (N)	2200 (≙ 15 bar)

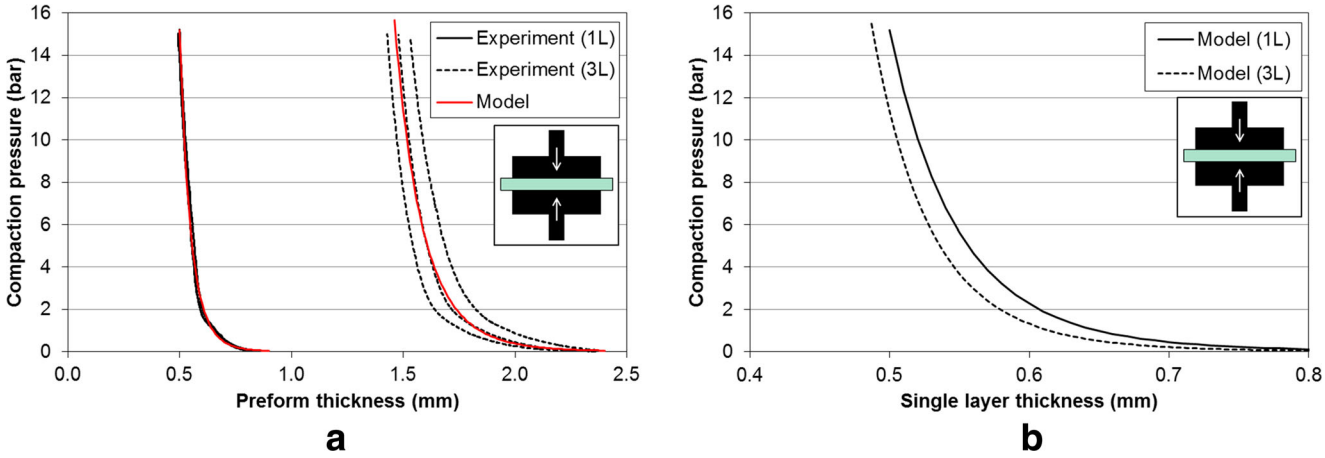

Fig. 13 Compressibility of single- (1 L) and multi-layer (3 L) preforms: (**a**) Measured and modeled preform compaction profiles; (**b**) Mean single layer thickness vs. compaction pressure

In this work, preform compaction tests are exemplarily performed on a chosen biaxial braided fabric. The tubular braid to be tested is draped and collapsed to a specific diameter and flattened width, respectively, considering the change of the interdependent braid parameters length, diameter or width and fiber angle [23, 26]. The flattened fabric is then cut in longitudinal direction and unfolded as depicted in Fig. 12b. A flat stack of braided fabrics is manually assembled and centrally positioned in the open gap of the test setup. A compressive load is then introduced to the preform via a constant motion of the crosshead. For each measurement, the compaction load F_c and the LVDT displacement is recorded until a predefined maximum compaction load is reached. The size of the flat specimen must exceed the dimensions of the compression plates in order to enable the calculation of the applied preform compaction pressure according to:

$$p_c = \frac{F_c}{A_c}. \tag{19}$$

Compaction behavior of braided preforms

The experimental work is focused on the investigation of the compaction behavior of a single layer (1 L) and a stack of three equally aligned layers (3 L) of a tubular braided sleeving (Table 2). The manually adjusted draping condition of the material is based on the situation of the preform inside the aforementioned tubular BARTM test rig, corresponding to an outer preform diameter of 21 mm. The resulting width and selected length of the flat test specimen is 66 and 80 mm, respectively, corresponding to the initial circumference and longitudinal dimension of the draped sleeving.

The compaction tests were conducted at room temperature using the relevant testing parameters summarized in Table 3. It is assumed that relaxation of the fiber network and thus time dependence of preform compaction can be neglected by choosing a relatively low compression rate. The minimum and maximum compressive load was selected to cover a wide range of preform compaction pressures relevant for BARTM. The measurements were repeated twice for each preform type.

The obtained preform compaction data is depicted in Fig. 13a. While the single-layer specimen demonstrates a consistent compression behavior, the repetitive measurements of the multi-layer preform show a significantly higher variability, which is attributed to nesting effects of the textile fabric [11, 12]. As a result, the theoretical single-layer thicknesses of the multi-layer preform exhibit decreased values in contrast to the compression profile of the single-layer preform (Fig. 13b).

The measurement data is fitted with the compaction model given in Eq. (14) using a least squares fit algorithm. The model adequately describes the measured compaction behavior, showing coefficients of correlation of 0.99 or higher for the single measurements. The resulting initial preform thickness $h_{p,\,0.1}$ as well as the model coefficients describing the mean compression behavior $p_c(h_p)$ for each preform type are specified in Table 4.

Results

In this section, the obtained models describing standalone bladder expansion and preform compaction are used to create an integral process window for the

Table 4 Resulting preform and compaction model parameters

Parameter	Preform 1 L	Preform 3 L
$h_{p,\,0.1}$ (mm)	0.809	2.238
$h_{p,\,1}$ (mm)	0.649	1.842
B	0.096	0.085

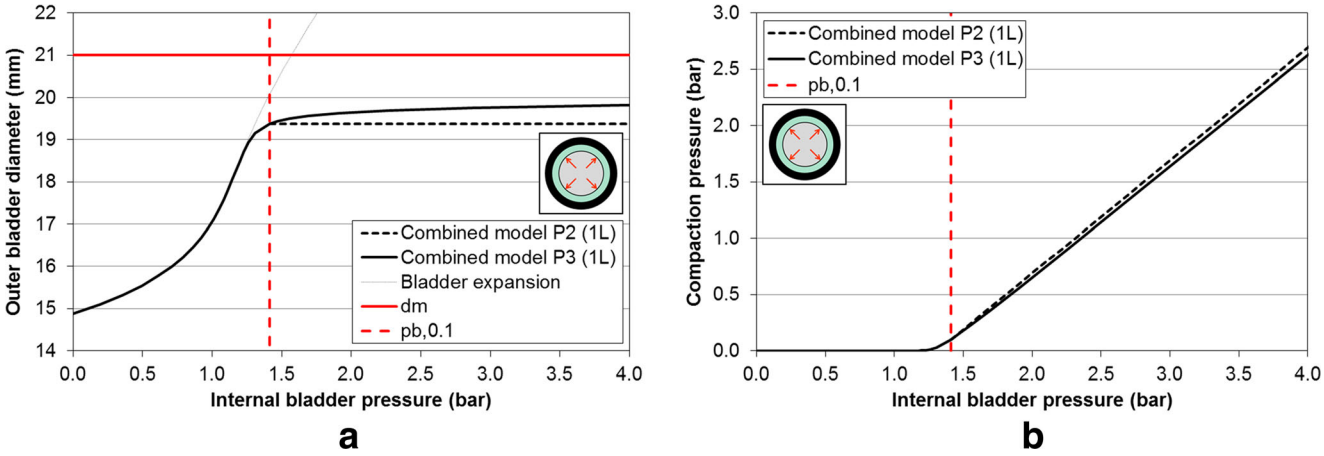

Fig. 14 Resulting process windows for the single-layer preform (1 L) based on the models P2 and P3 applicable for $p_b \geq p_{b,\ 0.1}$: (**a**) Outer bladder diameter and (**b**) preform compaction pressure vs. internal bladder pressure

combined expansion and compaction behavior according to the models P2 and P3 given by Eqs. (7) to (11). Again, it should be noted that these models are only valid in a defined preform compaction region corresponding to $p_b \geq p_{b,\ 0.1}$. Although they predominantly conform to the stand-alone tube expansion behavior for smaller internal bladder pressures, they cannot describe the region near the unknown pressure $p_{b,\ min}$, as this parameter can only be safely determined for an incompressible preform (model P1).

The following investigations are based on an exemplary tubular BARTM setup comprising an inner mold diameter d_m of 21 mm. The respective process windows for the single- and multi-layer preforms are depicted in Figs. 14 and 15. Here, the expansion and compaction behavior of model P3 in the range $p_b < p_{b,\ 0.1}$ was extrapolated for illustration purposes. The relevant pressure parameters $p_{b,\ 0.1}$ for full radial bladder expansion and minimum preform compaction ($p_{c,\ 0.1}$=0.1 bar) are determined according to Eqs. (7) to (9) and result in 1.41 bar for the single-layer braid and 0.98 bar for the multi-layer preform, corresponding to an outer bladder diameter $d_{b,\ 0.1}$ of 19.38 and 16.52 mm, respectively. The process windows clearly demonstrate that the multi-layer preform shows mold contact and thus compaction pressure build-up at lower bladder pressures as well as increased preform compressibility compared to the single-layer braid.

Based on the determined process models, the relevant local compaction pressures and preform thicknesses are now evaluated for an exemplary BARTM process, considering both the compaction and the subsequent resin injection stage through Eqs. (15) and (16). Similar to saturation experiments presented in a previous paper of the authors [8], a constant bladder and injection pressure of 4.0 and 1.5 bar, respectively, is used while the injection is performed at atmospheric pressure (p_f=0). According to Eq. (17), a valid preform compaction

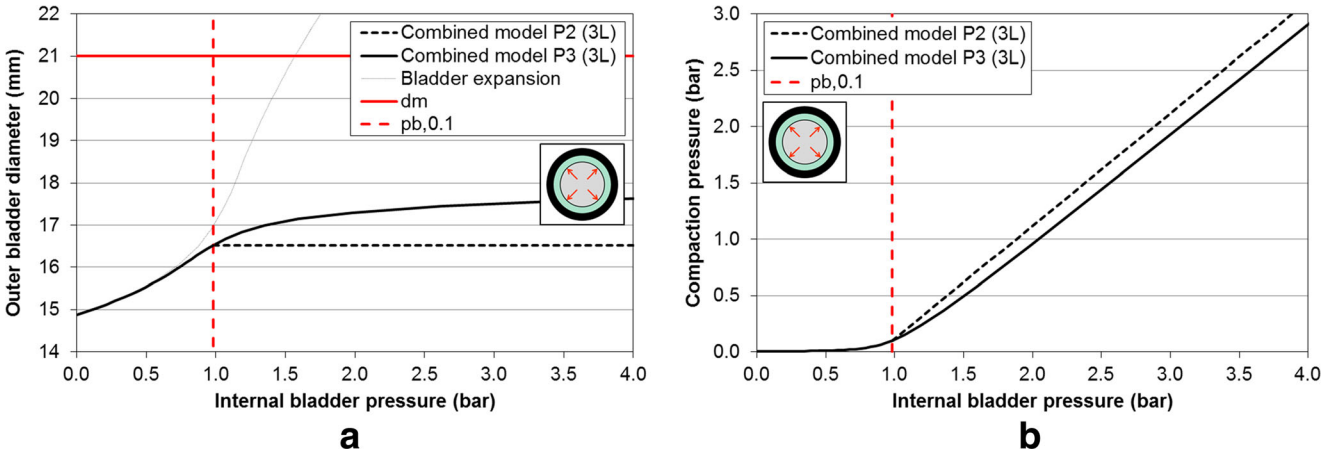

Fig. 15 Resulting process windows for the multi-layer preform (3 L) based on the models P2 and P3 applicable for $p_b \geq p_{b,\ 0.1}$: (**a**) Outer bladder diameter and (**b**) preform compaction pressure vs. internal bladder pressure

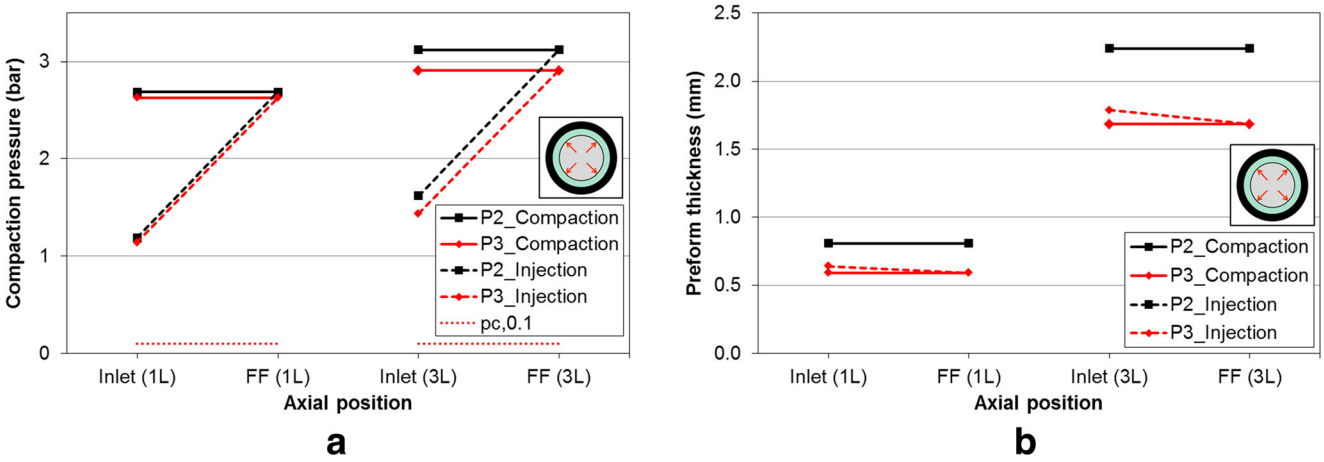

Fig. 16 Exemplary preform compaction data evaluated by model P2 and P3 for the single- (1 L) and multi-layer preform (3 L) during compaction and injection for $p_b/p_i/p_f$=4/1.5/0 bar: (**a**) Compaction pressure and (**b**) preform thickness for the respective axial positions of the BARTM setup (Inlet = injection gate, FF = flow front position)

pressure $p_c \geq p_{c,\ 0.1}$ is maintained throughout the injection process.

The resulting compaction data for the single- and multi-layer preforms is plotted for the relevant axial positions of the tubular BARTM setup, namely the fluid inlet and flow front position that corresponds to the outlet position at the end of the filling process (Fig. 16). For illustration purposes, the technically non-linear curves during resin injection are approximated through straight dashed lines. Regarding the compaction pressures it can be concluded that the influence of preform compressibility considered by model P3 is rather negligible for the single-layer preform, while the differences in compaction pressure between model P2 and P3 for the multi-layer preform are about 0.2 bar. If an evaluation of preform thicknesses is desired, then the application of model P3 should be preferred as model P2 obviously delivers only constant values that correspond to the initial preform thickness $h_{p,\ 0.1}$. Lastly, it is shown that the maintenance of a certain amount of preform compaction during injection significantly minimizes thickness evolution of the preform at the critical inlet position, as summarized in Table 5.

Table 5 Actual compaction pressure and preform thickness evolution Δh_p at the inlet position during resin injection according to model P3 in contrast to an injection procedure with minimum compaction pressure $p_c = p_{c,0.1}$

Parameter	Preform 1 L	Preform 3 L
Actual compaction pressure (bar)	1.14	1.44
Actual thickness evolution (mm)	0.049	0.103
Minimum compaction pressure (bar)	0.10	0.10
Maximum thickness evolution (mm)	0.217	0.555

Conclusions

This paper explored a methodology to determine the interdependent behavior of radial elastic bladder expansion and preform compaction during BARTM comprising an under-sized tubular bladder and a cylindrical mold. Different process models for incompressible and practically more relevant compressible preforms were presented based on available single-point or full compaction data. These models can be simply used to evaluate the preform compaction state (i.e. local compaction pressures and preform thicknesses) during BARTM. It is noteworthy that interaction effects between the expanding bladder and the textile preform (e.g. frictional forces) were neglected.

In order to consider the influence of the mechanical properties of reusable elastomeric bladders on preform compaction, an efficient optical testing method was proposed to directly measure the radial expansion behavior of silicone rubber tubes. It was shown that the Mullins effect, describing irreversible material stress-softening during repeated loading, has to be taken into account to enable reproducible bladder expansions, which was done by application of a defined preexpansion to a new bladder before first use. Obtained expansion measurement data, namely the pressure-dependent outer bladder diameters, was adequately fitted by means of a polynomial deformation model. Hence, this test rig can be used for a fast non-destructive characterization of a reusable tubular bladder prior to its use in BARTM.

The compression behavior of single- and multi-layer braided preforms was characterized by means of dry compaction measurements. Relaxation and lubrication effects, which can significantly affect preform compaction, were neglected for illustration purposes. As the thickness of an uncompacted compliant preform cannot be reasonably determined, the initial preform thickness was measured for a predefined

minimum compaction pressure, which can be chosen based on process requirements for the injection phase, e.g. to prevent flow-induced fiber displacement. Moreover, the full measurement data obtained for a relevant pressure range was successfully fitted to a power law-based preform compaction model.

It was shown that the separate material models describing bladder expansion and preform compaction can be used to create a combined process window for BARTM processing. By using exemplary process parameters, it was demonstrated that this approach enables the prediction of the local preform compaction pressure and thickness at the injection gate and flow front during the compaction and filling stage. In context with a previous paper of the authors [8], which explored the saturation behavior of tubular braided fabrics in the BARTM process, this work presented a procedure to evaluate the corresponding compaction pressure state during resin injection, particularly if under-sized elastomeric bladders are used.

Finally, it has to be noted that the validity and applicability of the coupled process model needs to be proven in future work. This requires the implementation of adequate online measurement methods that allow for an accurate determination of local preform compaction data and consider the complexity and accessibility of the tubular BARTM setup.

Acknowledgements Open access funding provided by Montanuniversität Leoben. The authors kindly acknowledge the financial support received from the Federal Ministry for Transport, Innovation and Technology (BMVIT) and the Austrian Research Promotion Agency (FFG) in frame of the programs “Intelligent Production” and “Production of the Future” within the respective research projects “Smart Composite Tube” (contract no. 838826) and “NovoTube” (contract no. 853453). Furthermore, the authors would like to thank the Chair of Materials Science and Testing of Polymers, Montanuniversität Leoben for their support with the preform compaction tests.

Compliance with ethical standards

Conflict of interest The authors declare that they have no conflict of interest.

References

1. Neitzel M, Mitschang P, Breuer U (2014) Handbuch Verbundwerkstoffe. Hanser, München
2. Hammami A, Al-Zarouni A (2001) Investigation of the RTM/Bladder Molding Process. In: Proceedings of the 13th International Conference on Composite Materials, Beijing, China. Open access: www.iccm-central.org
3. Ghiasi H, Lessard L, Pasini D, Thouin M (2010) Optimum structural and manufacturing Design of a Braided Hollow Composite Part. Appl Compos Mater 17(2):159–173. https://doi.org/10.1007/s10443-009-9106-6
4. Lehmann U, Michaeli W (1998) Cores lead to an automated production of hollow composite parts in resin transfer moulding. Compos Part A 29(7):803–810. https://doi.org/10.1016/S1359-835X(98)00007-4
5. Lehmann U (1999) Herstellung von endlosfaserverstärkten, hohlen Formteilen mit innendruckbeaufschlagten Kernen im Harzinjektionsverfahren. Verlag Mainz, Aachen
6. Chen B, Lang EJ, Chou T-W (2001) Experimental and theoretical studies of fabric compaction behavior in resin transfer molding. Mater Sci Eng A 317(1–2):188–196. https://doi.org/10.1016/S0921-5093(01)01175-3
7. Strohhäcker JB (2012) Herstellungsmethode für thermoplastische faserverstärkte Hohlkörperstrukturen. Verlag Mainz, Aachen
8. Schillfahrt C, Fauster E, Schledjewski R (2015) Optical Permeability Measurement on Tubular Braided Reinforcing Textiles. In: Proceedings of the 20th International Conference on Composite Materials, Copenhagen, Denmark. Open access: www.iccm20.org
9. Potter K (1997) Resin transfer moulding. Chapman & Hall, London. https://doi.org/10.1007/978-94-009-0021-9
10. Potluri P, Sagar TV (2008) Compaction modelling of textile preforms for composite structures. Compos Struct 86(1–3):177–185. https://doi.org/10.1016/j.compstruct.2008.03.019
11. Chen B (2000) Compaction of woven-fabric preforms. Compos Sci Technol 60(12–13):2223–2231. https://doi.org/10.1016/S0266-3538(00)00017-8
12. Lomov SV, Verpoest I, Peeters T, Roose D, Zako M (2003) Nesting in textile laminates. Compos Sci Technol 63(7):993–1007. https://doi.org/10.1016/S0266-3538(02)00318-4
13. Birkefeld K, Röder M, von Reden T, Bulat M, Drechsler K (2012) Characterization of biaxial and Triaxial braids. Appl Compos Mater 19(3–4):259–273. https://doi.org/10.1007/s10443-011-9190-2
14. Robitaille F, Gauvin R (1998) Compaction of textile reinforcements for composites manufacturing. II Polym Compos 19(5):543–557. https://doi.org/10.1002/pc.10128
15. Robitaille F, Gauvin R (1999) Compaction of textile reinforcements for composites manufacturing. III Polym Compos 20(1):48–61. https://doi.org/10.1002/pc.10334
16. Yenilmez B, Senan M, Murat Sozer E (2009) Variation of part thickness and compaction pressure in vacuum infusion process. Compos Sci Technol 69(11–12):1710–1719. https://doi.org/10.1016/j.compscitech.2008.05.009
17. Chen B, Cheng A-D, Chou T-W (2001) A nonlinear compaction model for fibrous preforms. Compos Part A: Appl Sci Manuf 32(5):701–707. https://doi.org/10.1016/S1359-835X(00)00148-2
18. Lekakou C, Johari MAKB, Bader MG (1996) Compressibility and flow permeability of two-dimensional woven reinforcements in the processing of composites. Polym Compos 17(5):666–672. https://doi.org/10.1002/pc.10658
19. Bezerra R, Wilhelm F, Strauß S, Ahlborn H (2015) Manufacturing of Complex Shape Composite Parts through the Combination of Pull-Braiding and Blow Moulding. In: Proceedings of the 20th International Conference on Composite Materials, Copenhagen, Denmark. Open access: www.iccm20.org
20. Fong L, Liu B, Advani SG (1995) Modeling and Simulation of Resin Transfer Molding with Flexible Mold Walls. In: Proceedings of the Composites Institute’s 50th Annual Conference, Cincinnati, USA
21. Correia NC, Robitaille F, Long AC, Rudd CD, Šimáček P, Advani SG (2005) Analysis of the vacuum infusion moulding process.

Compos Part A 36(12):1645–1656. https://doi.org/10.1016/j.compositesa.2005.03.019
22. Goncharova G, Cosson B, Deléglise Lagardère M (2015) Analytical modeling of composite manufacturing by vacuum assisted infusion with minimal experimental characterization of random fabrics. J Mater Process Tech 219:173–180. https://doi.org/10.1016/j.jmatprotec.2014.12.010
23. Schillfahrt C, Schledjewski R (2017) Analytical modeling of textile parameters and draping behavior of 2D biaxial braided Sleevings. Polym Polym Compos 25(5):315–326
24. Mohammed U, Lekakou C, Dong L, Bader M (2000) Shear deformation and micromechanics of woven fabrics. Compos Part A 31(4):299–308. https://doi.org/10.1016/S1359-835X(99)00081-0
25. Yüksekkaya ME (2001) Analysis of elastic deformation of braided tubular structures for medical applications. J Eng Sci 7(2):277–285
26. Li S, Tsai S, Lee LJ (2000) Preforming analysis of biaxial braided fabrics Sleeving on pipes and ducts. J Compos Mater 34(6):479–501. https://doi.org/10.1177/002199830003400603
27. Liu XL, Falzon PJ, Sweeting R, Paton R (2004) Effective compressibility and permeability of multi-layer non-crimp fiberglass reinforcements. J Reinf Plast Compos 23(8):861–879. https://doi.org/10.1177/0731684404033378
28. Li L, Zhao Y, Yang J, Zhang J, Duan Y (2015) An experimental investigation of compaction behavior of carbon non-crimp fabrics for liquid composite molding. J Mater Sci 50(7):2960–2972. https://doi.org/10.1007/s10853-015-8860-0
29. Kastanis D, Steiner H, Fauster E, Schledjewski R (2015) Compaction behavior of continuous carbon fiber tows. Adv Manuf Polym Compos Sci 1(3):169–174
30. Modi D, Johnson M, Long A, Rudd C (2009) Analysis of pressure profile and flow progression in the vacuum infusion process. Compos Sci Technol 69(9):1458–1464. https://doi.org/10.1016/j.compscitech.2008.05.026
31. Parnas RS, Schultheisz CR, Ranganathan S (1996) Hydrodynamically induced preform deformation. Polym Compos 17(1):4–10. https://doi.org/10.1002/pc.10585
32. Endruweit A, Gehrig S, Ermanni P (2003) Mechanisms of Hydrodynamically induced in-plane deformation of reinforcement textiles in resin injection processes. J Compos Mater 37(18):1675–1692. https://doi.org/10.1177/0021998303035182
33. Simacek P, Heider D, Gillespie JW, Advani S (2009) Post-filling flow in vacuum assisted resin transfer molding processes. Compos Part A 40(6–7):913–924. https://doi.org/10.1016/j.compositesa.2009.04.018
34. Timms J, Bickerton S, Kelly PA (2012) Laminate thickness and resin pressure evolution during axisymmetric liquid composite moulding with flexible tooling. Compos Part A 43(4):621–630. https://doi.org/10.1016/j.compositesa.2011.12.012
35. Rudd CD (1997) Liquid moulding technologies. SAE International, Warrendale. https://doi.org/10.1533/9781845695446
36. Diani J, Fayolle B, Gilormini P (2009) A review on the Mullins effect. Eur Polym J 45(3):601–612. https://doi.org/10.1016/j.eurpolymj.2008.11.017